DFT study of NHx (x = 1−3) Adsorption on RuO2(110) surfaces

ARTICLE *in* THE JOURNAL OF PHYSICAL CHEMISTRY C · DECEMBER 2009

Impact Factor: 4.77 · DOI: 10.1021/jp8062355

DFT Study of NH_x ($x = 1-3$) Adsorption on $RuO_2(110)$ Surfaces

Chia-Ching Wang, Ya-Jen Yang, and Jyh-Chiang Jiang*

Department of Chemical Engineering, National Taiwan University of Science and Technology, 43 Keelung Road, Section 4, Taipei, 106, Taiwan

Received: July 15, 2008; Revised Manuscript Received: November 17, 2008

We have used density functional theory (DFT) to investigate the adsorption of NH_x species ($x = 1-3$) onto $RuO_2(110)$ surfaces at various monolayer coverages and onto oxygen-rich $RuO_2(110)$ surfaces. We characterized the structures, vibrational frequencies, and detailed bonding interactions between the adsorbates and the surfaces. The binding energy increased as the number of hydrogen atoms bonded to the N atom decreased, i.e., $NH_{3\text{-cus}}$ binds most weakly to the surface, whereas NH_{cus} has the highest binding energy. We investigated the nature of the metal$-NH_x$ bonding through analyses of the density of states (DOS) and electron density difference contour maps. The DOS analysis allowed us to characterize the state interactions between the NH_x species and the surface; the electron density difference maps provided evidence that was consist with the DOS analysis. A greater number of state interactions led to the higher binding energy of an NH_x species: for $NH_{3\text{-cus}}$ bound through a single σ bond, the binding energy was 1.56 eV; it increases to 4.23 eV when two π bonds were present in the NH_{cus} bonding mode. In addition, hydrogen bonding played an important role in the binding of $NH_{3\text{-cus}}$ and NH_{cus}, especially for the weakly coordinated $NH_{3\text{-cus}}$. The formation of hydrogen bonds was evident from changes in the bond length and stretching frequency of the N−H bonds.

Introduction

The decomposition of ammonia (NH_3) is an important industrial reaction. The catalytic oxidation of NH_3 to NO, the so-called Ostwald process, is a key step in the production of nitric acid. In addition, the oxidation of NH_3 leading to N_2 and H_2O has become of increasing interest in connection with the removal of NH_3 from waste streams.[1] Another potentially important application of NH_3 is its use as a hydrogen source and storage substance for fuel cells.[2−4] Because of these and other technological, economical, and environmental factors, a large number of reports have described the decomposition and oxidation reactions of NH_3.[5−8] The most critical factor in determining the reactivity and selectivity of these reactions is the nature of the catalyst. Several materials have been investigated as catalysts for NH_3 dissociation reactions, including metals,[5,6] alloys,[7] and metal oxides.[8,9]

The $RuO_2(110)$ surface, depicted schematically in Figure 1, exhibits high catalytic activity for CO oxidation.[10−14] The surface presents exposed rows of 2-fold coordinated oxygen atoms (O_{br}), 5-fold coordinated Ru atoms (Ru_{cus}; cus = coordinatively unsaturated site), and triply coordinated layer oxygen atoms (O_{3f}), all along the [001] direction. Additional oxygen atoms may be adsorbed on top of the Ru_{cus} atoms (so-called O_{cus}) through further exposure to O_2. The Ru_{cus} atoms on the surface behave as catalytically active sites onto which NH_3 or O_2 molecules are adsorbed from the gas phase. In 2005, Wang et al.[8] investigated the selective oxidation of NH_3 to either N_2 or NO on $RuO_2(110)$ single-crystal surfaces. They found that the concentration of oxygen atoms adsorbed on these Ru_{cus} sites determined both the reactivity and selectivity of the NH_3 oxidation process. Surprisingly, they obtained almost 100% selectivity for NO formation on $RuO_2(110)$ at 530 K, a temperature much lower than those applied in the typical Ostwald process with Pt-based catalysts (>1100 K).

Although the structures of NH_3 and NH_2 on $RuO_2(110)$ surface have been characterized expermimentally,[8] no detailed studies (e.g., the assignment of vibrational frequencies and the detailing coverage effect) of the bonding of NH_x species on such surfaces have been reported previously. In this paper, we present the data obtained from density functional theory (DFT) simulations of the binding of NH_x species onto $RuO_2(110)$ surfaces. We investigated the binding of NH_x species at various monolayer surface coverages and on oxygen-rich $RuO_2(110)$ surfaces. We characterized the details of the interactions between NH_x species and the surfaces by analyzing the density of states (DOS), the electron density differences, and the vibrational frequencies. Our calculated vibrational frequencies are in good agreement with the known experimental results.[8]

Computational Details

All DFT calculations were performed with the Vienna Abinition Simulation Package (VASP).[15−19] The generalized gradient approximation (GGA) was used with the functional described by Perdew and Wang[20] and a cutoff energy of 300 eV. Electron−ion interactions were investigated with use of the projector augmented wave method;[21] spin-polarized calculations were performed for all of the structural optimizations. After structural optimization, a normal-mode frequency analysis was conducted to check the validity of the optimized geometries. The $RuO_2(110)$ surface was modeled as a two-dimensional slab in a three-dimensional periodic cell. The [001], [$\bar{1}$10], and [110] directions of the slab were defined as the x, y, and z dimensions of the supercell. The slab was a 2×1 surface having the thickness of five layers, where one layer is defined as one O−Ru−O repeat unit. A 12.8 Å vacuum space was introduced in the z direction to curtail interactions between the slabs. For this (2×1)-$RuO_2(110)$ surface model, the k-points of $3 \times 3 \times 1$ were set by Monkhorst−Pack.

* To whom correspondence should be addressed. E-mail: jcjiang@mail.ntust.edu.tw. Phone: +886-2-27376653. Fax: +886-2-27376644.

10.1021/jp8062355 CCC: $40.75
Published on Web 01/27/2009

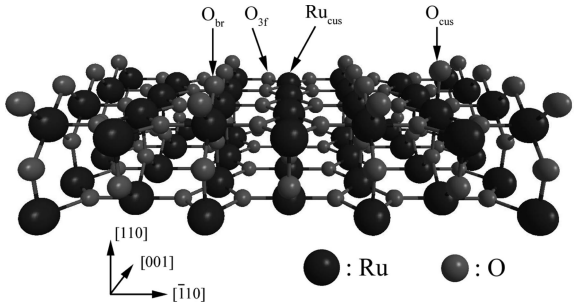

Figure 1. Ball and stick model of the stoichiometric $RuO_2(110)$ surface.

The binding energy (E_b) of each NH_x species was calculated by using the formula

$$E_b = \frac{(E_{surf} + nE_A) - E_{A/surf}}{n} \quad (1)$$

where E_{surf} is the energy of the stoichiometric surface or the oxygen-rich surface, E_A is the energy of a single NH_x molecule, and $E_{A/surf}$ is the total energy of the NH_x molecule adsorbed on the surface. For different coverages, n indicates the number of bonded NH_x molecules. A positive value of E_b indicates an exothermic chemisorption process. The electron density difference (Q_{diff}) was calculated in a manner similar to the calculation of the binding energy:

$$Q_{diff} = Q_{A/surf} - (Q_{surf} + Q_A) \quad (2)$$

where Q_{diff} is the difference at each grid point in the total electron density matrix between that of the NH_x-bonded surface ($Q_{A/surf}$) and that of the sum of the surface (Q_{surf}) and the single NH_x molecule (Q_A). According to this definition, positive and negative values of Q_{diff} correspond to increasing and decreasing electron densities, respectively.

Results

1. NH_x on the Stoichiometric $RuO_2(110)$ Surface. Parts a–c of Figure 2 display the geometries of the NH_x species ($x = 1-3$) bound to the stoichiometric $RuO_2(110)$ surface with coverage of 0.5 ML; Tables 1 and 2 list the binding energies and related structural parameters of the bonded species, respectively. The NH_3 molecule binds to the surface through donation of its lone pair of electrons to a surface Ru_{cus} atom. The calculated binding energy of the NH_3 molecule on the surface is 1.56 eV; the bond length between the Ru and N atoms, d(Ru–N), is 2.16 Å. The molecular axis of the adsorbed $NH_{3\text{-}cus}$ molecule was not aligned normal to the surface because of hydrogen bonding between $NH_{3\text{-}cus}$ and a surface O_{br} atom; this strong attractive force—between an H atom on $NH_{3\text{-}cus}$ and the O_{br} atom—causes the $NH_{3\text{-}cus}$ unit to incline slightly toward the O_{br} atom. The length of this hydrogen bond was 2.14 Å; the length of the hydrogen-bonded N–H bond was 1.04 Å. The strength of the Ru–N bond increased upon decreasing the number of H atoms on the N atom. After removing one H atom from $NH_{3\text{-}cus}$, the binding energy of $NH_{2\text{-}cus}$ on the $RuO_2(110)$ surface increased significantly (to 2.47 eV). For NH_{cus}, the binding energy on the surface was 4.23 eV. The values of d(Ru–N) decreased dramatically upon increasing the bond order of Ru–N: 1.93 Å for $NH_{2\text{-}cus}$ and 1.77 Å for NH_{cus}. The binding of $NH_{2\text{-}cus}$ to the surface was close to that of an sp^2 hybrid structure. The normal of the $NH_{2\text{-}cus}$ plane was aligned in the [1̄10] direction. Thus, the two N–H bonds of $NH_{2\text{-}cus}$ point in the [001] direction and do not form hydrogen bonds with O_{br} atoms. For NH_{cus}, hydrogen bonding again induced an attractive lateral force that caused the NH_{cus} molecule to tilt toward the O_{br} atoms, resulting in a tilt angle of 13.5° and a hydrogen bond length of 1.92 Å.

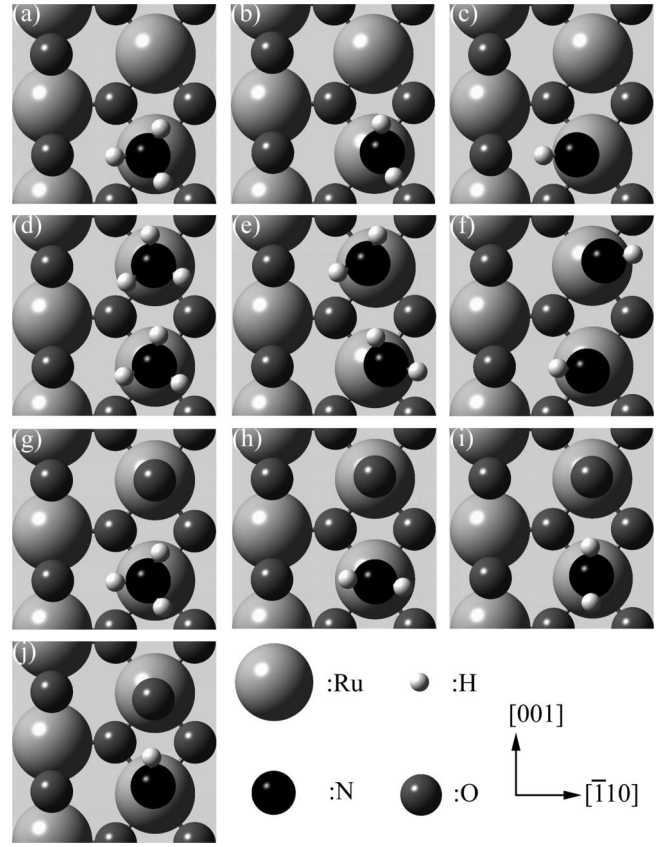

Figure 2. Top views of NH_x species adsorbed onto $RuO_2(110)$ surfaces: (a–c) $\theta = 0.5$ ML; (d–f) $\theta = 1$ ML; (g–j) oxygen-rich surface.

TABLE 1: Binding Energies (eV) of NH_x Species on Stoichiometric $RuO_2(110)$ Surfaces ($\theta = 0.5$ or 1 ML) and Oxygen-Rich $RuO_2(110)$ Surfaces

species	$\theta = 0.5$ ML	$\theta = 1$ ML	oxygen-rich
$NH_{3\text{-}cus}$	1.56	1.13	1.86
$NH_{2\text{-}cus}$	2.47	2.39	2.45 (I)
			2.42 (II)
NH_{cus}	4.23	4.25	4.29

TABLE 2: Structural Parameters (Å) for NH_x Molecules Bound to $RuO_2(110)$ Surfaces ($\theta = 0.5$ ML)

	$NH_{3\text{-}cus}$	$NH_{2\text{-}cus}$	NH_{cus}
d(N–H)	1.03	1.03	
	1.03	1.03	
d(N–H)$_{br}$[a]	1.04		1.07
d(Ru–N)	2.16	1.93	1.77
d(O_{br}···H)	2.14		1.92

[a] Hydrogen atom bonded to O_{br} atom.

Parts d–f of Figure 2 display the binding geometries of NH_x molecules onto the surfaces at coverages of 1 ML; Table 1 lists the binding energies. Increasing the coverage did not significantly affect the average binding energies of the $NH_{2\text{-}cus}$ and NH_{cus} systems. The geometry of NH_{cus} was similar to that at a coverage of 0.5 ML; in contrast, the geometry of $NH_{2\text{-}cus}$ at 1 ML was quite different from that at a coverage of 0.5 ML. As revealed in Figure 2e, the bonded $NH_{2\text{-}cus}$ system at high coverage exhibits an sp^3-hybridized structure and forms two intermolecular hydrogen bonds (N–H···N and N–H···O_{br}).

TABLE 3: Structural Parameters (Å) for NH_x Molecules Bound on Oxygen-Rich RuO_2(110) Surfaces

	$NH_{3\text{-cus}}$	$NH_{2\text{-cus}}$	NH_{cus}
$d(N-H)_{br}$[a]	1.04	1.03 (I)	
$d(N-H)_{cus}$[b]	1.03	1.03 (II)	1.05
d(Ru−N)	2.17	1.92 (I)	1.75
		1.92 (II)	
$d(O_{br}\cdots H)$	2.16	2.64 (I)	
$d(O_{cus}\cdots H)$	2.31	2.32 (II)	1.87

[a] Hydrogen atom bonded with O_{br} atom. [b] Hydrogen atom bonded with O_{cus} atom.

Although at high coverage the adsorbed $NH_{2\text{-cus}}$ molecule contains two additional hydrogen bonds not present at low coverage, the binding energy of each $NH_{2\text{-cus}}$ decreased to 2.39 eV; this phenomenon is due to the special electronic structure of $NH_{2\text{-cus}}$ on the surface, which we discuss in the next section. At high coverage, the binding energy of each $NH_{3\text{-cus}}$ molecule decreased from 1.56 to 1.13 eV.

2. NH_x on Oxygen-Rich RuO_2(110) Surfaces. In the oxygen-rich RuO_2(110) surface, one of the Ru_{cus} sites of the 2 × 1 surface is occupied by an O atom and the other features an adsorbed NH_x species. Tables 1 and 3 list the binding energies and some structural parameters, respectively; parts g−j of Figure 2 display the binding geometries. The binding energies of $NH_{2\text{-cus}}$ and NH_{cus} did not change significantly when O_{cus} atoms were present on neighboring sites, but the binding energy of $NH_{3\text{-cus}}$ increased dramatically (to 1.86 eV) because one more hydrogen bond (length: 2.31 Å) could form with an O_{cus} atom in this system. We found two possible binding structures for $NH_{2\text{-cus}}$ on the oxygen-rich surface, with the $NH_{2\text{-cus}}$ unit maintaining its sp^2-hybridized structure. We assigned these two $NH_{2\text{-cus}}$ structures on the oxygen-rich surface as structures I (Figure 2h) and II (Figure 2i), respectively. The molecular planes of these two adsorbed $NH_{2\text{-cus}}$ units are aligned normal to the [001] and [$\bar{1}$10] planes, respectively. The binding energies of geometries I and II were 2.45 and 2.42 eV, respectively. For NH_{cus} bound to the oxygen-rich surface, the N−H bond changed direction from that observed for the stoichiometric surface to point at the O_{cus} atom. Relative to the situation for NH_{cus} on the stoichiometric surface at a coverage of 0.5 ML, the binding energy of 4.29 eV on the oxygen-rich surface was slightly higher and the value of $d(O_{cus}\cdots H)$ was shorter than that of $d(O_{br}\cdots H)$, implying a stronger interaction between the O_{cus} atoms and the NH_{cus} molecules on the oxygen atom-rich surface.

3. Vibrational Frequencies. We calculated the vibrational frequencies for the NH_x species with $\theta = 0.5$ ML on both the stoichiometric and oxygen-rich RuO_2(110) surfaces. Table 4 lists the calculated frequencies of the N−H stretching modes (υ(N−H)) and deformation modes (δ) and of the Ru−N stretching modes (υ(Ru−N)). For the binding of $NH_{3\text{-cus}}$, the three υ(N−H) frequencies were 392.4, 418.4, and 425.2 meV. Because of the hydrogen bonding interaction with the surface bridge oxygen atom, the υ(N−H) frequency at 392.4 meV was red-shifted significantly compared with the other two. We observed such significant red-shifts for the value of υ(N−H) in the binding of both the $NH_{3\text{-cus}}$ and NH_{cus} molecules. For $NH_{3\text{-cus}}$ on the oxygen-rich surface, the hydrogen-bonded υ_s(N−H) frequency was 398.7 meV; the values of υ(N−H) for the binding of NH_{cus} on the two different surfaces were 359.8 (stoichiometric surface) and 380.2 meV (oxygen-rich surface), respectively. Although the binding structures I and II both exist with short distances $d(O_{br}\cdots H)$ and $d(O_{cus}\cdots H)$ for the $NH_{2\text{-cus}}$ system on the oxygen-rich surface, the NH stretching frequencies all remained higher than 400 meV. The values of υ(N−H) of $NH_{2\text{-cus}}$ on the stoichiometric surface were 416.1 and 430.2 meV; on the oxygen-rich surface, they ranged from 404.1 to 429.0 meV. These simulated results are in good agreement with experimental data[8] for the values of υ_s(N−H) and υ_a(N−H) for $NH_{3\text{-cus}}$ on the stoichiometric surface (403 and 418 meV, respectively) and on the oxygen-rich surface (404 and 420 meV, respectively). The simulated NH deformation modes that we calculated for $NH_{3\text{-cus}}$ also compare very well with experimental data: Wang et al.[8] reported that the experimental values of δ_s and δ_a for $NH_{3\text{-cus}}$ were 149 and 199 meV, respectively, on the stoichiometric surface; we obtained simulated values of 147.5 (δ_s), 198.4 (δ_a), and 199.2 (δ_a) meV.

TABLE 4: Vibrational Frequencies (meV) of NH_x Species Adsorbed on Stoichiometric ($\theta = 0.5$ ML) and Oxygen-Rich RuO_2(110) Surfaces

species	mode[a]	$\theta = 0.5$ ML	oxygen-rich	exptl[b]
$NH_{3\text{-cus}}$	υ_s(N−H)	392.4	398.7	403 (404)
	υ_a(N−H)	418.4	413.7	418 (420)
		425.2	420.5	
	δ_s	147.5	152.9	149 (154)
	δ_a	198.4	194.1	199 (199)
		199.2	201.3	
	υ(Ru−N)	48.4	51.5	
$NH_{2\text{-cus}}$	υ_s(N−H)	416.1	413.0 (I)	
			404.1 (II)	
	υ_a(N−H)	430.2	429.0 (I)	
			424.3 (II)	
	δ_s	187.9	181.9 (I)	(186)
			184.0 (II)	
	υ(Ru−N)	75.9	75.5 (I)	
			76.0 (II)	
NH_{cus}	υ(N−H)	359.8	380.2	
	υ(Ru−N)	102.5	105.6	

[a] υ_s and υ_a, symmetric and asymmetric stretching modes; δ_s and δ_a, symmetric and asymmetric deformation modes. [b] From ref 8. The energies were recorded during the NH_3 oxidation reactions on the oxygen-rich surface; the energies in parentheses are the values obtained for NH_x species adsorbed on the oxygen-rich surface.

The trend in the values of the Ru−N stretching modes of NH_x on the RuO_2(110) surfaces was relatively simple. The υ(Ru−N) frequencies of $NH_{3\text{-cus}}$, $NH_{2\text{-cus}}$, and NH_{cus} on the stoichiometric surface were 48.4, 75.9, and 102.5 meV, respectively; on the oxygen-rich surface, they were 51.5, 75.5 (76.0), and 105.6 meV, respectively. Thus, the υ(Ru−N) frequencies increased upon increasing the Ru−N bond strength.

Discussion

According to their recent TPD experiments, Wang et al. reported[8] that the desorption temperature for $NH_{3\text{-cus}}$ on an RuO_2(110) surface is 420 K. This temperature is significantly higher than those for NH_3 on Ru(11$\bar{2}$1) (300−350 K)[22] and Ru(001) (310 K)[23] surfaces. Moreover, the calculated binding energy of 1.56 eV for $NH_{3\text{-cus}}$ on a RuO_2(110) surface is higher than those on other metal surfaces: 0.71 eV on Pt(111),[24] 0.79 eV on Pt(100),[25] 0.94 eV on Pt(211),[25] 0.47 eV on Fe(110),[26] 0.95 eV on Fe(111),[26] and 0.75 eV on Rh(111).[6] For NH_3 molecules to adsorb onto a metal surface, the major bonding force is the dative bond formed to the surface metal atom. On the RuO_2(110) surface, however, additional hydrogen bonding between the NH_3 molecule and the surface O atoms increases the attractive force. As indicated in Figure 2a, for NH_3 adsorbed onto the RuO_2(110) surface, one of the hydrogen atoms interacts with a surface O_{br} atom and forms a strong hydrogen bond (length 2.14 Å). Because the strength of the N−H bond weakens

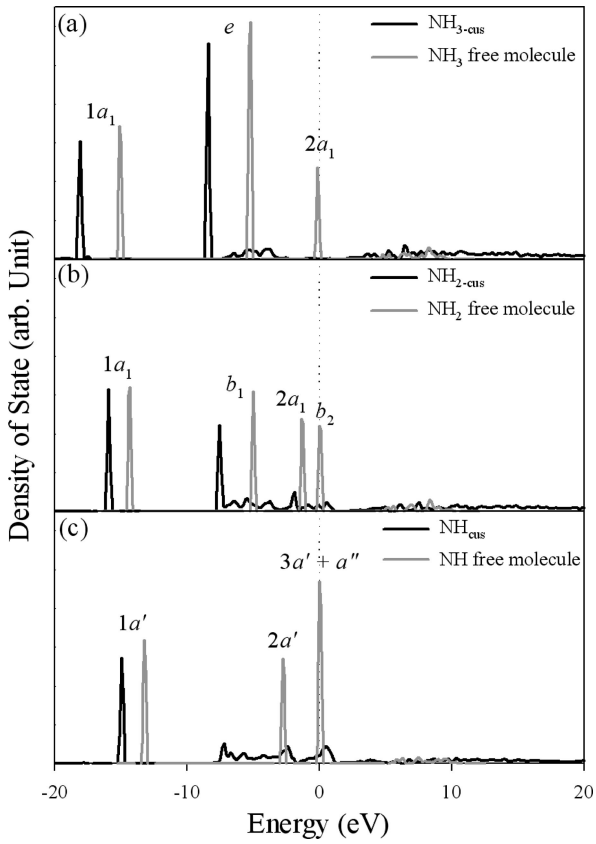

Figure 3. DOS of NH_x molecules before (gray line) and after (black line) binding to the RuO_2(110) surface. The assignment of each hybrid state was based on the specific symmetry of $NH_{x\text{-cus}}$: (a) NH_3, C_{3v}; (b) NH_2, C_{2v}; and (c) NH, C_s. The Fermi level was located at 0 eV (dotted line).

as a result of such hydrogen bonding, a significant red-shift (to 392.4 meV) occurred to the value of υ(N−H). For the NH_3 adsorption process at $\theta = 1$ ML, steric effects caused the N−H···O_{br} hydrogen bond to become distorted; i.e., because no N−H bonds could point in the [$\bar{1}$10] direction, the hydrogen bonding strength decreased and, therefore, so too did the binding energy of $NH_{3\text{-cus}}$. The binding energy of $NH_{3\text{-cus}}$ at high coverage was 1.13 eV, i.e., less than that of $NH_{3\text{-cus}}$ at low coverage by 0.43 eV. Moreover, because of the decrease in the strength of the hydrogen bond, all of the N−H stretching frequencies in the high-coverage system were greater than 400 meV. In contrast, for the NH_3 molecules adsorbed on the oxygen-rich surface, the additional hydrogen bond increased the binding energy to 1.86 eV. A similar phenomenon (i.e., hydrogen bond-stabilized adsorption) has been observed for the adsorption of NH_3 on Au(111) surfaces; e.g., the adsorption of NH_3 to the Au(111) surface is exothermic by only 0.05 eV, but it increases to 0.38 eV when preadsorbed O atoms are present.[27] This stabilization also arose from hydrogen bonding, with donor−acceptor pairs forming in the NH_3···O substructure. In addition to stabilizing the $NH_{3\text{-cus}}$ molecules on the RuO_2(110) surface, the stronger hydrogen bonds weakened the strength of the N−H bonds; we suspect that this phenomenon is responsible for the high rate of NH_3 oxidation on the surface.

To analyze the bonding nature of the NH_x species on the RuO_2(110) surface, we plotted the DOS distribution. Figure 3 presents the DOS of the NH_x molecules before (gray line) and after (black line) binding to the surface at $\theta = 0.5$ ML. In Figure 3a, we observe that the $1a_1$ and e states of NH_3 were stabilized after adsorption, whereas the $2a_1$ state became dispersed after interaction with the surface. The vanishing of the sharp $2a_1$ state was due to the interaction with the d_{z^2} state of Ru_{cus} and the formation of the σ bond between $NH_{3\text{-cus}}$ and Ru_{cus}. Figure 4a displays the detailed interaction between the $2a_1$ and d_{z^2} states. The black and gray lines represent the distributions of the d states in the Ru_{cus} atom and the states of NH_x species, respectively; the dashed and solid lines represent the systems before and after the adsorption of NH_x, respectively. For the bonding between $NH_{3\text{-cus}}$ and the surface, we observe a significant delocalization of the $2a_1$ state, ranging from −7 to 4 eV; the unique d_{z^2} state had also shifted to a higher energy level.

For the stronger bound $NH_{2\text{-cus}}$, we observed one more state interaction from the DOS analysis. In Figure 3b, the $2a_1$ and b_2 states of $NH_{2\text{-cus}}$ are dispersed; the $1a_1$ and b_1 states are stabilized. As mentioned above, the $NH_{2\text{-cus}}$ units on the RuO_2(110) surface at $\theta = 0.5$ ML possessed sp^2-hybridized structures. The double bond character of the bond between $NH_{2\text{-cus}}$ and Ru_{cus} resulted from interactions between the $2a_1$ and d_{z^2} states and between the b_2 with d_{yz} states, i.e., σ and π bonds to the surface, respectively. Parts b and c of Figure 4 present the detailed state interactions. The state interaction of $2a_1$ in Figure 4b is similar to the bonding of $NH_{3\text{-cus}}$ in Figure 4a because they feature the same type of σ bonding. In contrast, a smaller range of state splitting appears in Figure 4c because of a weaker π interaction. The double bond character plays an important role in determining the binding energy of $NH_{2\text{-cus}}$. When the coverage of $NH_{2\text{-cus}}$ increased to 1 ML, the sp^2-hybridized character decreased to form a more sp^3-hybridized structure. This structural change was reflected in the reduced π bond character of the Ru−N bond. The average binding energy of $NH_{2\text{-cus}}$ at $\theta = 1$ ML was 2.39 eV, which is lower than the corresponding value of 2.47 eV at $\theta = 0.5$ ML; in addition, the value of d(Ru−N) of 1.96 Å at $\theta = 1$ ML was longer than that at $\theta = 0.5$ ML. In the binding system for $NH_{2\text{-cus}}$ at $\theta = 1$ ML, the greater sp^3 character of the $NH_{2\text{-cus}}$ molecules would lead to more hydrogen bonding interactions (N−H···O_{br} and N−H···N), which we would expect to stabilize the bonded molecules; nevertheless, the binding energy of $NH_{2\text{-cus}}$ at $\theta = 1$ ML was lower than that at $\theta = 0.5$ ML. This result implies that the π bonding interaction was the major factor affecting the binding energy of $NH_{2\text{-cus}}$.

Figure 3c displays the DOS before and after the binding of the NH molecule onto the RuO_2(110) surface. The three sharp states 2a′, 3a′, and a″ were delocalized in NH_{cus}; we could identify only the N−H bonding state 1a′. Relative to the situation for $NH_{2\text{-cus}}$, the binding energy increased dramatically because of the presence of one more π bond between the NH_{cus} unit and the surface, i.e., π interactions between the $2a'$ state and the surface d_{yz} state and between the a″ state and the d_{xz} state. Parts d−f of Figure 4 depict the state interactions. In the binding of NH_{cus}, the increased strength of π bonding led to an enormous increase in the binding energy to 4.23 eV; the high binding energy in this system arose not only from the Ru−N bond but also from hydrogen bonding. The hydrogen bonding of NH_{cus} on the surface was stronger than that of $NH_{3\text{-cus}}$, as evidenced from a comparison of the values of d(N−H), d(O_{br}···H), and υ(N−H). For the adsorption of NH_{cus}, the values of d(N−H), d(O_{br}···H), and υ(N−H) were 1.07 Å, 1.92 Å, and 359.8 meV, respectively; for $NH_{3\text{-cus}}$, they were 1.04 Å, 2.14 Å, and 392.4 meV, respectively. For the binding of NH_{cus} on the oxygen-rich RuO_2(110) surface, the N−H bond changed direction and pointed toward the O_{cus} atom. This change caused the binding energy to increase from 4.23 to 4.29 eV. Therefore, we believe that the rotation of 90° along the Ru−N bond did not change the bonding force of Ru−N, but the increase in binding energy

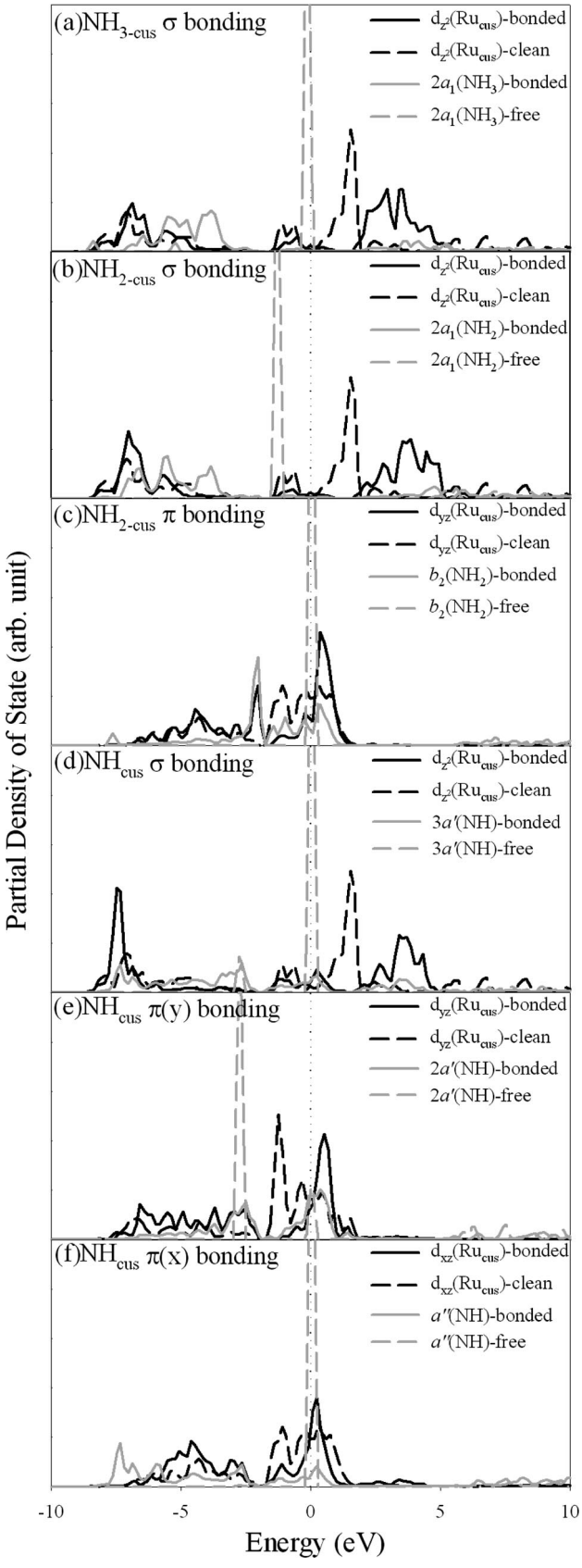

Figure 4. PDOS of the *d* orbital in Ru_{cus} (black line) and the NH_x molecular hybrid states (gray line) for Ru_{cus}−N bonding at $\theta = 0.5$ ML after NH_x adsorption: (a) σ bonding of $NH_{3\text{-cus}}$; (b) σ bonding of $NH_{2\text{-cus}}$; (c) π bonding of $NH_{2\text{-cus}}$; (d) σ bonding of NH_{cus}; (e) π bonding of NH_{cus} in the *y* direction; and (f) π bonding of NH_{cus} in the *x* direction. The dashed and solid lines represent the distribution of orbitals before and after adsorption. The Fermi level was located at 0 eV (dotted line).

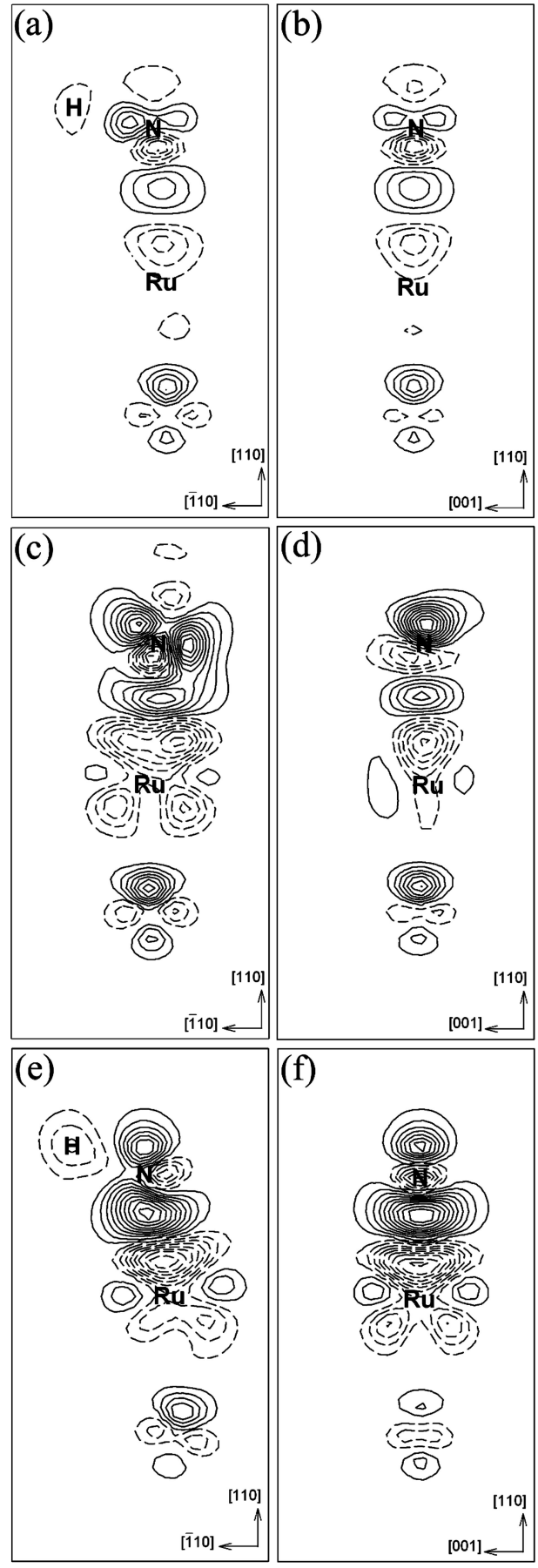

Figure 5. Electron density difference contour plots of NH_x ($x = 1-3$) at $\theta = 0.5$ ML: (a, b) $NH_{3\text{-cus}}$; (c, d) $NH_{2\text{-cus}}$; and (e, f) NH_{cus}. The solid and dashed lines represent increasing and decreasing electron densities, respectively.

presumably arose from the change in hydrogen bonding because the value of $d(O_{cus}\cdots H)$ of 1.87 Å is shorter than that of $d(O_{br}\cdots H)$. Nevertheless, no matter whether the N−H bond of NH_{cus} points toward the O_{br} atom or the O_{cus} atom, the energy difference was only 0.08 eV; therefore, both structures for NH_{cus} adsorption should exist in real systems.

Another approach toward characterizing the bonding of NH_x species on $RuO_2(110)$ surfaces is through analysis of their electron density difference contour plots. We plotted the electron density difference contour maps for $NH_{3\text{-}cus}$, $NH_{2\text{-}cus}$, and NH_{cus} on the stoichiometric surface at $\theta = 0.5$ ML (Figure 5). The two-electron difference planes are aligned normal to the [001] and [$\bar{1}$10] directions and cut through the NH_x-bonded Ru_{cus} atom. An increase in the electron density area (solid line) between N and Ru_{cus} appears in each contour plot; the area increases in the order from $NH_{3\text{-}cus}$ to NH_{cus}, which is consistent with the trend in the binding energy. In the electron density difference contour of $NH_{2\text{-}cus}$ (Figure 5c), we observe a d-type electron density loss on the Ru_{cus} atom; similarly, for the NH_{cus}-bonded Ru_{cus}, d-type electron density loss also occurs (Figure 5e,f). These d-type electron density losses are in line with the PDOS (projected density of state) analysis. The electron density loss in Figure 5c coincides with the π interaction between $NH_{2\text{-}cus}$ and the d_{yz} state of Ru_{cus} in Figure 4c. In addition, parts e and f of Figure 5 are consistent with parts e and f of Figure 4, respectively, which indicates the π bonding of NH_{cus} with d_{yz} and d_{xz}, respectively. The loss of electron density in these d states can be justified through consideration of the PDOS analysis in Figure 4. Prior to binding the $NH_{2\text{-}cus}$ and NH_{cus} molecules, the d states of Ru_{cus} in parts c, e, and f of Figure 4 were distributed around the Fermi level (black dashed line); after the adsorption of $NH_{2\text{-}cus}$ and NH_{cus} (black solid line), however, these d states became localized and were located beyond the Fermi level. Thus, π bonding caused part of the d_{xz} or d_{yz} state to cross the Fermi level and shift to a higher energy state; this situation also resulted in the electron density losses in Figure 5c,e,f.

Conclusion

DFT calculations revealed decreases in the values of d(Ru−N) and increases in the values of υ(Ru−N) and the orbital interactions between Ru_{cus} and N, which led to increased binding energies, upon decreasing the number of H atoms in NH_x systems. The change in bond order between the NH_x species and the surface Ru_{cus} was clearly evident from analyses of the DOS and electron density difference contours. As each successive H atom was removed, one additional π bond formed between the N and Ru_{cus} atoms. As a result, we observed signals for one π bond for $NH_{2\text{-}cus}$ and two π bonds for NH_{cus} in the corresponding DOS diagrams and electron density difference contour maps. This electronic analysis—combining DOS and electron density differences—revealed the detailed nature of the bonding of NH_x species onto $RuO_2(110)$ surfaces. In addition, we found that hydrogen bonding interactions play an important role in increasing the binding energy for the adsorption of $NH_{3\text{-}cus}$ and NH_{cus}. On the basis of our analysis of the calculated vibrational frequencies, the large red-shifts in the values of υ(N−H) of the surface-bound $NH_{3\text{-}cus}$ and NH_{cus} molecules, relative to those of the free species, revealed the presence of strong $N-H\cdots O_{br}$ and $N-H\cdots O_{cus}$ hydrogen bonding interactions. In contrast, because hydrogen bonding did not influence the adsorption of $NH_{2\text{-}cus}$ to any significant extent, we found that the bonding of $NH_{2\text{-}cus}$ to the surface was determined primarily by the strength of the π bond between the Ru_{cus} and N atoms. The calculated vibrational frequencies also revealed that there was no significant red-shift in the value of υ(N−H) for the $NH_{2\text{-}cus}$ molecules; they were all greater than 400 meV.

Acknowledgment. We thank the National Science Council of Taiwan for supporting this research financially (NSC 94-2120-M-011-001 and 95-2113-M-011-001) and the National Center of High-Performance Computing and the Institute of Nuclear Energy Research, Atomic Energy Council, Taiwan, for computer time and facilities.

References and Notes

(1) Gang, L.; Anderson, B. G.; van Grondelle, J.; van Santen, R. A.; van Gennip, W. J. H.; Niemantsverdriet, J. W.; Kooyman, P. J.; Koester, A.; Brongersma, H. H. *J. Catal.* **2002**, *206*, 60.
(2) Busca, G.; Lietti, L.; Ramis, G.; Berti, F. *Appl. Catal., B* **1998**, *18*, 1.
(3) van Hardeveld, R. M.; van Santen, R. A.; Niemantsverdriet, J. W. *J. Vac. Sci. Technol. A* **1997**, *15*, 1558.
(4) Stolbov, S.; Rahman, T. S. *J. Chem. Phys.* **2005**, *123*, 204716–1.
(5) Imbihl, R.; Scheibe, A.; Zeng, Y. F.; Güenther, S.; Kraehnert, R.; Kondratenko, V. A.; Baerns, M.; Offermans, W. K.; Jansen, A. P. J.; van Santen, R. A. *Phys. Chem. Chem. Phys.* **2007**, *9*, 3522.
(6) Popa, C.; Offermans, W. K.; van Santen, R. A.; Jansen, A. P. J. *Phys. Rev. B* **2006**, *74*, 155428.
(7) Moran, E.; Cattaneo, C.; Mishima, H.; de Mishima, B. A. L.; Silvetti, S. P.; Rodriguez, J. L.; Pastor, E. *J. Solid State Electrochem.* **2008**, *12*, 583.
(8) Wang, Y.; Jacobi, K.; Schöne, W.-D.; Ertl, G. *J. Phys. Chem. B* **2005**, *109*, 7883.
(9) McGrill, P. R.; Idriss, H. *Langmuir* **2008**, *24*, 97.
(10) Over, H.; Kim, Y. D.; Seitsonen, A. P.; Wendt, S.; Lundgren, E.; Schmid, M.; Varga, P.; Morgante, A.; Ertl, G. *Science* **2000**, *287*, 1474.
(11) Fan, C. Y.; Wang, J.; Jacobi, K.; Ertl, G. *J. Chem. Phys.* **2001**, *114*, 10058.
(12) Kim, Y. D.; Over, H.; Krabbes, G.; Ertl, G. *Top Catal.* **2001**, *14*, 95.
(13) Wang, J.; Fan, C. Y.; Jacobi, K.; Ertl, G. *J. Phys. Chem. B* **2002**, *106*, 3422.
(14) Over, H.; Muhler, M. *Prog. Surf. Sci.* **2003**, *72*, 3.
(15) Kresse, G.; Hafner, J. *Phys. Rev. B* **1993**, *47*, 558.
(16) Kresse, G.; Hafner, J. *Phys. Rev. B* **1993**, *48*, 13115.
(17) Kresse, G.; Hafner, J. *Phys. Rev. B* **1994**, *49*, 14251.
(18) Kresse, G.; Furthmüller, J. *Comput. Mater. Sci.* **1996**, *6*, 15.
(19) Kresse, G.; Furthmüller, J. *Phys. Rev. B* **1996**, *54*, 11169.
(20) Perdew, J. P. In *Electronic Structure of Solids '91*; Ziesche, P., Eschrig, H., Eds.; Akademie Verlag: Berlin, Germany, 1991; p 11.
(21) Kresse, G.; Joubert, D. *Phys. Rev. B* **1999**, *59*, 1758.
(22) Jacobi, K.; Wang, Y.; Fan, C. Y.; Dietrich, H. *J. Chem. Phys.* **2001**, *115*, 4306.
(23) Benndorf, C.; Madey, T. *Surf. Sci.* **1983**, *135*, 164.
(24) Offermans, W. K.; Jansen, A. P. J.; van Santen, R. A. *Surf. Sci.* **2006**, *600*, 1714.
(25) Offermans, W. K.; Jansen, A. P. J.; van Santen, R. A.; Novell-Leruth, G.; Ricart, J. M.; Pérez-Ramírez, J. *J. Phys. Chem. C* **2007**, *111*, 17551.
(26) Satoh, S.; Fujimoto, H.; Koboyashi, H. *J. Phys. Chem. B* **2006**, *110*, 4846.
(27) López, N.; García-Mota, M.; Gómez-Díaz, J. *J. Phys. Chem. C* **2008**, *112*, 247.

JP8062355